Leveraging the DPK Combustion Instabilities Characteristics to Optimize Gas Turbine Lean Premixed Combustor Performance

Wilson Alli, Osagie Ighodalo, Christopher Ajuwa

Abstract— This paper discusses the identification of Dual Purpose Kerosene (DPK) induced combustion instabilities occurrence characteristics towards the optimisation of lean premixed combustor performance in gas turbine engines.The process involves the identification of crucial combustion instability instigators associated with DPK fuel. The computational fluid dynamics (CFD) technology using the ANSYS Fluent code (Academic Research CFD) version 16.2 was adopted to numerically investigate the characteristic of DPK fuel combustion during combustion or thermoacoustic instabilities occurrence on lean-burn equivalence ratios. An AutoCAD pre-designed combustor was exported to the ANSYS Fluent GUI for fine tuning, gridding/mesh generation process with the ANSYS Fluent solver, leveraging the finite difference method (FDM) to solve emerging discretised complex non-linear equations. With established boundary conditions contiguous to an operational industrial gas turbine engine generating at 20MW, simulations were conducted on both the steady-state and transient combustion regimes to evolve details of DPK fuel combustion mannerism profiles on simulation convergence attainment. Details of dynamic pressure, total pressure and, temperature plots under four equivalence ratios (0.3, 0.5, 0.7 and 0.9)ϕ were subsequently analysed to obtain parameters contingent to designing a fuel specific GTE LP Combustor Wireless Sensor Technology/ Supervisory Control and Data Acquisition (WST/SCADA) system and MRO schedule for the GTE.

Index Terms - DPK, ANSYS Fluent, finite difference method, SCADA, WST, Computational Fluid Dynamics, GTE

u

1 INTRODUCTION

The stringent environmental regulations on gas turbines original equipment manufacturers (OEMs) on pollution control requirements precipitated the advent of the lean premixed combustion technology geared toward the elimination of various kinds of oxides of Nitrogen (NO_x), Sulphides(SO_x), unburned hydrocarbons (UHC) and other pollutants from gas turbine effluents from the environment. The successes attained at curbing the pollutants in gas turbine emissions precipitated the debilitating combustion phenomenon commonly referred to as combustion instabilities. Contemporary gas turbine engines operate with the lean premixed (LP) combustors as result of their capability to operate under lower combustion temperatures. This capability renders the LP combustors highly susceptible to combustion instabilities occurrence due to the excitation and coupling of the combustor's acoustic modes with the unsteady heat release waves of the combustion flowfields. This results in the oscillations of the flowfields leading to severe structural vibrations of the combustor systems with catastrophic impact on the machine resulting in damages to the combustor systems, turbine guide vanes and blades (Figures 1 and 2). The phenomenon occurrences cascade to frequent and high MRO costs, early plant or machine decommissioning and high operational downtime. Contemporary Gas Turbines operate across a wide range of fuels that consists of paraffin, naphthenes and aromatic types of hydrocarbons and the ratios of the fuel compounds which defines the fuel properties are primarily dependent on the crude type, and these properties must respectively conform to required standards. The hydrocarbon contents of fuel characterise the fuel physical, chemical properties and consequentially defining the fuel combustion characteristics and its propensity to the occurrence of combustion instabilities.

The frequency of failures of gas turbine engines equipped with the lean premixed combustor system is astronomically high, and this has been a matter of grave concern to owners and operators in the power and energy industries. The consequences of the equipment failure and its non-availability have a spiralling effect on the equipment reliability, remediation costs, operational downtime with costs overrun. This ultimately precipitates negative consequences in the organisation 's annual returns [18].

The Combustion instabilities arise from the resonant interactions within the premixed combustors leading to oscillations of the flowfield thereby inducing several undesirable effects: large-amplitude pressure and velocity oscillations resulting in thrust oscillations and structural vibrations, increased heat fluxes at the combustor walls, flashback and flame blowoff [1]; [6]; [25];[7].

The resonant interactions are induced by a feedback loop between the oscillatory combustion process and one of the combustors natural acoustic modes. (Figure 3). This phenomenon's inducing mechanics was qualitatively

described by [21] as combustion instability occurs when the acoustic waves gain energy when the unsteady rate of heat input is in phase with pressure oscillations within the combustor.

Several authors on gas turbine combustion have postulated the nexus between the composition of fuel types, combustion reactions and kinetics and equivalence ratios variation to combustion instabilities occurrences in gas turbine engines [10]; [1]; [19]; [11].

[1] argued that the performance of combustion system depend strongly on the physical and chemical properties of the fuels as it impacts the combustion dynamics through flame type formation, heat release rate with the eventual incensement of the acoustic waves and inducing the feedback mechanism that establishes the instabilities. In another instance,[23] argued on the futility of designing a combustor that would be stable during the entire operating range of the gas turbine or to predict the operating condition at which a given combustor would be unstable. This, according to him, is due to the limited understanding of the fundamentals of combustion instability. [23] further stated that the development of the next generation lean premixed gas turbine (LPGT) Combustor would require design tools that would be based entirely on stability models to enable it to show the relationship between combustor design, operating ranges and combustion instability.

Figure 1: Damages on Combustor Liner and Turbine Blades by combustion Instabilities. Lieuwen and Yang (2006)

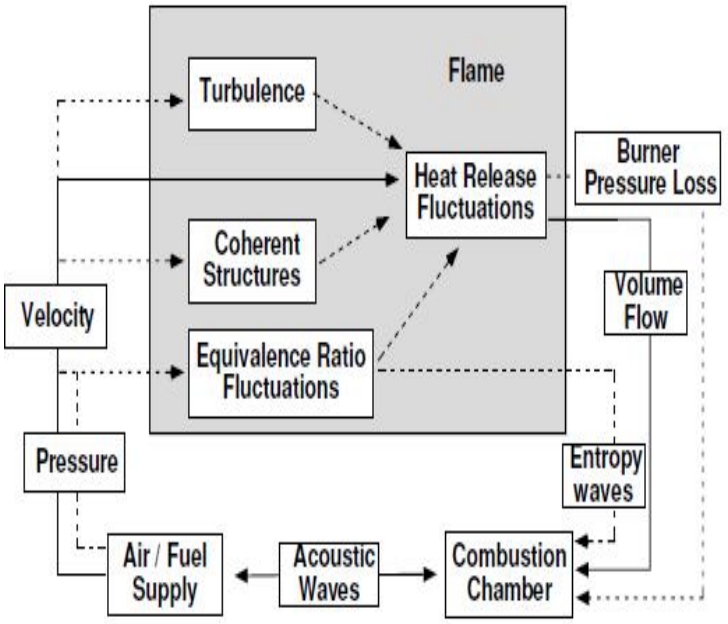

Figure 2: Burner Assembly(Left) damaged by combustion instability and new burner assembly(right)

Figure 3. Interactions between flow, acoustics and heat release in a Combustion system. Source: Polifke, (2004)

In Nigeria, the gas turbine engines are widely deployed to generate power for the national grid, and this is increasing geometrically, as the country strives to expand the current power generating capacity from 5000MW to 20,000MW in the immediate future. The reliance on fossil-fueled powered engines is mainly due to the ready availability of the fuel type in commercial scale in the country. In meeting with power sufficiency in the country, massive investment in power infrastructures, centred on the construction of power generation facilities is expected. Currently, 75% of the generated power in Nigeria is predominantly fossil-fueled gas turbine engines power plants, and these engines acquisition trend would continue in the quest to meet the immediate power sufficiency goal of the government. However, enhancing the availability and reliabilities of the GTEs, and avoiding early engine decommissioning, become a top-priority, and this would require specific domestication of critical skill-sets in lean premixed combustor design optimisation and management[22]

2 MATERIALS AND METHOD

2.1 Materials

- ANSYS Fluent (Academic Research CFD) version 16.2
- The simulation was carried out on an Intel (R) Core (TM) i-3-2377M CPU @ 1.7 GHz, 6BG memory RAM.
- Transient state is calculated until residues lower than 10^{-3} for all the variables except for the equation of energy (<10^{-6}). A constant time step size (s) of 1 second and numbers of time step of 2500 with 20 max iterations/time step.
- CHEMKIN Collection, Release 3.6 providing gas-phase diffusivities
  GRI-Mech 3.0 Gas-phase kinetic mechanism
  POLIMI Kinetic Mechanism for liquid formation.

2.2 Methods

2.2.1 Simulation setup

Since the theme of investigation is premised around combustion, fluid flow and heat transfer the ANSYS Fluent (Academic Research CFD) Version 16.2 was selected as the tool for the simulation and analysis of the earlier mentioned parameters, and the CFD codes targets solution to the main flow governing equations.

The process entails simulation of DPK (kerosene) in lean premixed gas turbine swirl stabilised combustor. This entails conducting the simulation at a power output of 20000KW (20MW) on a two-dimensional Planar (2-D space)

2.2.2 Simulation stepwise process

STEP 1. Creating Fluid flow analysis system on the ANSYS Workbench

STEP 2. Launch the design Modeller Program

STEP 3. A Pre-development of a 2-D model of typical gas turbine annular combustor using AutoCAD was undertaken (Figure 4). The AutoCAD model of the combustor was exported into the simulation environment created by ANSYS Design Modeller(ADM).The nominal length of the combustor is 800mm, width 200mm, the air and fuel enters into the combustor separately and are premixed by the swirler which is positioned at an angle of 50 degrees to the air and fuel flow. The Swirler consist of 8 vanes. The fuel was injected into the combustion chamber through the nozzle

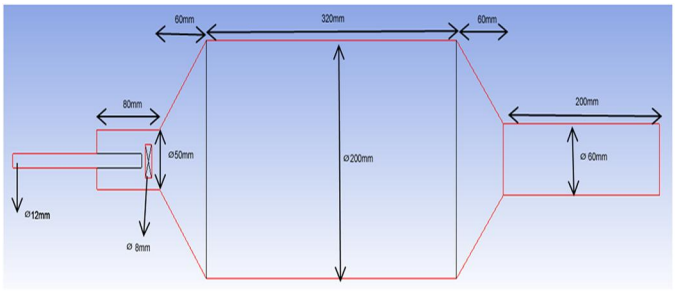

Figure 4: LP Combustor Dimensions

STEP 4. Geometric model preparation

The Computational Domain (LP combustor) was developed using the AutoCAD software with the following configuration (Figure 1) and exported to the ANSYS Fluent (Academic Research CFD) v.16.2 GUI for meshing (Figures 5). The model preparation was premised on a geometrical drawing of the combustors and mesh construction, and it played a significant role in the simulation accuracy and the solution convergence through its accuracy and stability of the numerical computation. A 2-D Axis symmetric mesh with 24,834 faces, 12,168 quadrilateral cells of mesh quality of 5.80670e-01 maximum orthogonal skew, and minimum orthogonal quality of 4.13782e-01 was adopted for the simulation (Figure 5).

Launching of the Meshing programme for the Grid/Mesh generation process through setting the Relevance Centre to Medium(RCM) under sizing and the midsize element nodes. The mesh generation process presented the following details in Tables 1 and 2

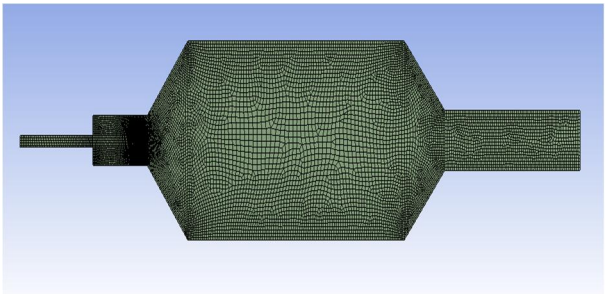

Figure 5: Layout of Meshed LP Combustor

Table 1: Simulation Set-Up Details

Models	Function Description of Governing Parameters adopted for the Investigation
Solver	Pressure based, absolute velocity formulation, transient time bases simulation
Model	k – epsilon equation – standard model,
	Radiation – discrete ordinate,
Spark ignition (for gas fuel only)	Initial radius – 0.0002, location – 0.169104, 0.0234036,
Acoustic	Broadband noise sources
scaled residuals	10-6 for all the equations
species	Transport model, Chemistry interaction – eddy dissipation concept, volumetric reaction coupled with a CHEMKIN option to allow for significant species of combustion reactions
Kinetics reaction mechanism.	Kinetic reaction mechanism of the Gas Research Institute (GRI) mechanism (Gas fuel), and POLIMI Kinetic mechanisms (Liquid fuel) both in Chemkin format
Scheme	Couple
Discretization	Gradient –Least square cell base
	Pressure - Second Order Upwind
	momentum – second order Upwind
	others – first order upwind
Solution control	Default
Initialization	Standard
Calculation	Time step size – 0.00001, numbers of time step = 500, max iteration = 20
Mesh Scale	X-min(mm) -172, X- max(mm) 696
	Y-min(mm) -2.8715e-31, Y-max(mm) 198.926
Total Volume(m^3)	1.02E-01
Face Area Statistics	Minimum face area (m2): 5.090730e-04
	Maximum face area(m2): 1.010023e-02

Table 2: LP Combustor Mesh Generation Statistics

Method	Triangles	Definitions
Sizing	Size function = proximity	
	relevance = fine	
	smoothing = fine	
Volume statistics (m^3)	minimum volume (m3): 6.035354e-08,	Total volume (m3): 1.016065e-01
	maximum volume (m3): 5.777815e-05	
Face area statistics (m^2)	minimum face area (m2): 2.008038e-04	
	maximum face area (m2): 9.971539e-03	
Mesh Quality	Minimum Orthogonal Quality = 4.13782e-01	Orthogonal Quality ranges from 0 to 1, where values close to 0 correspond to low quality.
	Maximum Ortho Skew = 5.80670e-01	Ortho skew ranges from 0 to 1, where values close to 1 correspond to the low quality
Maximum Aspect Ratio	7.26E+00	
Cells	12168	
Faces	24834	
Nodes	12666	

STEP 5. Setting Up Flow Domain through the launching of Fluent Fluid Flow (FFF) programme

STEP 6. Defining and setting the Boundary Conditions through default Domain in the Outline – Two inlets (fuel, air) Air mass flow rate, Inlet air temperature, Inlet total pressure of air, Inlet static pressure of air. The mass flow rate of fuel, Inlet fuel temperature, Inlet total pressure of the fuel. The velocity of fuel injection, Outlet Temperature, Pressure loss, Combustion efficiency, with Combustor walls added. Defined Combustion fuel kinetic mechanism equations for either Gas

Fuel/Liquid fuel as per CHEMKIN and POLIMI. Both were sourced for explicit hydrocarbon oxidation and pyrolysis. The GRI-Mech 3.0 provided the gas-phase kinetic mechanism for the carbon species with gas diffusivities obtained from CHEMKIN with other fuel variables(viscosities and thermal conductivities)

Table 3: Boundary conditions

Type	Properties
Fuel inlet	Diameter (mm) = 15mm, Gas fuel (Temperature 15^{0}C (288K), pressure = 101325 P) Liquid fuel (Temperature 25^{0}C (298K), pressure = 101325 P)
Air Inlet	Diameter (mmm) = 50mm, Gas fuel Temperature 15^{0}C (288K), pressure = 101325 P Liquid fuel (Temperature 25^{0}C (298K), pressure = 101325 P
Outlet	Diameter (m) = 0.06, Static pressure = 0
Wall (Air)	Material = steel
Wall (Fuel)	Material = steel
Wall (Combustor)	Material = steel
Wall (Outlet)	Material = steel
Wall (Swirler)	Material = steel

- Model $\kappa - \varepsilon$ Turbulent model
- Motion/Fluid Type (Swirler Configuration)

N = VRe/D^2, Where N = Rotational speed in Rev/Sec, V = Kinematics viscosity (M^2/S), Re = Reynolds number, D = impeller diameter. V = μ/ϱ where μ = absolute or dynamic viscosity (NS/m^2), ϱ = density (Kg/m^3) Re< 23000 – Laminar, 2300 < Re < 4000 - Transition, Re>4000 – Turbulence

Table 4: Initial Conditions of Fuels Investigated

Fuel	DPK
Impeller diameter D (m)	0.008
Kinematics viscosity V @ 15^{0}C M^2/S	2.71 x 10^{-6}
Rotational speed N Rev/Sec	1.355
Rotational speed (N * 2π) Rad/Sec	8.513
Fuel inlet diameter (m)	0.015
Air inlet diameter (m)	0.10

D = 0.008, D^2 = 0.000064

STEP 7. Analysis /Solution Setup – ANSYS Fluent (Academic Research CFD) v.16.2

The mass flow of air and that of the fuels were found using equations (3.1) and (3.2) respectively at an output power of 20000KW(20MW). This enables the details as in Tables (5) respectively for each fuel type.

$$\dot{m}_{fuel} = {}^{P(KW)}/_{LHV_{fuel}} \text{ X } 1000 \quad (3.1)$$

$$\dot{m}air = {}^{\dot{m}_{fuel}}/_{MW_{fuel}\Phi}/_{MW_{air}Xn_{stoich}} \quad (3.2)$$

Where P is the Power output, LHV_{fuel} represent the Lower Heating Value of fuel, ϕ is the combustion equivalence ratio,n_{air} is the mole amount in stoichiometric-fuel-air combustion. The amount of simulations was limited to different premixed air-fuel ratios($\dot{m}_{air}/\dot{m}_{fuel}$) and MW is the molecular weight of fuel.

Table .5: Parameters for DPK Fuel-Air Flow Combustion at 20MW

Kerosene(DPK)

ϕ	M_{fuel} kg/s	M_{air} kg/s	M_{air}/M_{fuel}	FAR	Power Output KW
0.3	0.464037	4.4515153	9.593018014	0.104242481	20,000
0.5	0.464037	2.66709191	5.747584589	0.17398613	20,000
0.7	0.464037	1.908837	4.113544825	0.243099332	20,000
0.9	0.464037	1.48201625	3.193745865	0.313111951	20,000

STEP 8: Discretization by Solver (Process detailing)

The next step of the simulation analysis entails the initialisation and the solution control processes within the CFD Solver. This involves resolution of the discrete values of the flow properties. Such properties as velocity, pressure-temperature including other transport parameters must be initialised within the solver to enable the calculation of the solution to the governing equation.

It is well perceived that the governing equations remain the cornerstone of fluid flow dynamics and the Navier-Stokes govern the fluid flowfield, and Euler Equations expressed in partial differential equations(PDE)

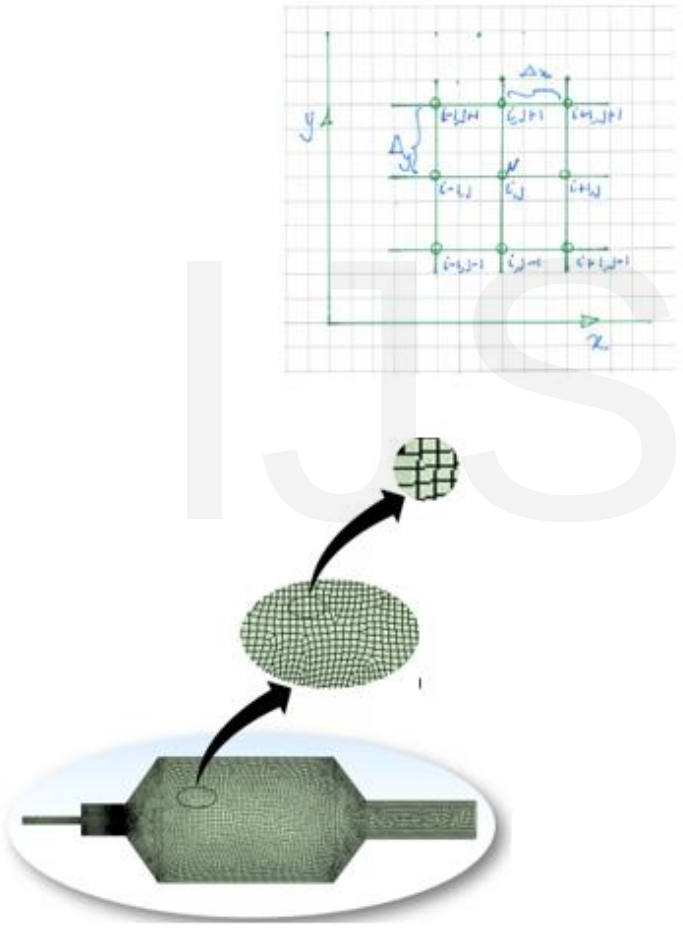

Figure: 6: Section of LP Combustor for discretisation process

It is known that an analytical solution to the PDEs would provide a closed expression for the flowfield variables, u, v, p, ϱ etc. as functions of *x* and *y*, are used to give values to the flowfield variables at any given point within the flow. Figure 5. presents the domain in meshed format, with 24,834 faces, 12,168 quadrilateral cells and 12,666 nodes.

At the commencement of the discretization, a procedure which entails the replacement of the PDEs in the fluid flow governing equations by approximate algebraic difference quotients expressed in the flowfield variables at points in the grid system, then the PDEs would then have been replaced entirely by a system of algebraic equations which are then solved for the values of the flowfield variables. This procedure of discretising the governing equation is by the finite difference method.

In this wise Figure 5 (see domain inset) above about a grid point *N*(*i, j)* and the flowfield variable *u* (velocity) determination about the grid point denotes the *x* component of velocity at point *i, j*, then the velocity u *i*+1,*j* at point (*i*+1,*j)* can be expressed in terms of Taylor's series expanded about nodal point N (*i,j*) as detailed below

$$ui+1,j = ui,j + \left(\frac{\partial u}{\partial x}\right)_{i,j}\Delta x + \left(\frac{\partial^2 u}{\partial x^2}\right)_{i,j}\frac{(\Delta x)^2}{2} + \left(\frac{\partial^3 u}{\partial x^3}\right)_{i,j}\frac{(\Delta x)^3}{6} + \cdots \quad (3.3)$$

To obtain a higher accuracy, additional higher order terms must be included in the RHS of the equation. This equation constitutes an exact expression for the velocity *u* about point i, j, i.e. *ui*+1,*j* and solving the equation above to obtain (Tu et al., 2013)

$$\left(\frac{\partial u}{\partial x}\right)_{i,j} = \frac{ui+1,j-ui,j}{\Delta x} - \left(\frac{\partial u}{\partial x}\right)_{i,j}\frac{\Delta x}{2} - \left(\frac{\partial^3 u}{\partial x^3}\right)_{i,j}\frac{(\Delta x)^2}{6} + \cdots \quad (3.4)$$

Finite-difference. Truncation error

The first term on the RHS represents the finite-difference representation of the partial derivative, while the last terms constitute the truncation error.

Next step involves the approximation of the partial derivative with the above algebraic difference quotient and shows that ;

$\left(\frac{\partial u}{\partial x}\right)_{i,j} \approx \frac{ui+1,j-ui,j}{\Delta x}$ This expression is referred as first-order accurate, which is better expressed as

$$\left(\frac{\partial u}{\partial x}\right)_{i,j} = \frac{ui+1,j-ui,j}{\Delta x} O(\Delta x) \quad (3.5)$$

now referred to the first-order-forward difference as it only applies to information of the RHS of the grid-point *(i,j)* implying that it uses u*i*+1, *j* and ui,j.

To expand the information on the LHS of (i,j), we write a Taylor series expansion of ui-1, j about *ui, j*

$$ui-1,j = ui,j + \left(\frac{\partial u}{\partial x}\right)_{i,j}(-\Delta x) + \left(\frac{\partial^2 u}{\partial x^2}\right)_{i,j}\frac{(-\Delta x)^2}{2} + \left(\frac{\partial^3 u}{\partial x^3}\right)_{i,j}\frac{(-\Delta x)^3}{6} + \cdots \quad (3.6)$$

Solving for $\left(\frac{\partial u}{\partial x}\right)_{i,j}$ we obtain

$$\left(\frac{\partial u}{\partial x}\right)_{i,j} = \frac{ui,j-u-1j}{\Delta x} O(\Delta x) \quad (3.7)$$

This is the backward difference

In CFD, the first order accuracy is widely known to be insufficient to construct a finite difference quotient of second order-order accuracy. To attain this status (second-order accuracy), equation (3.7) is subtracted from (3.3) as follows to obtain

$$ui + 1, j = ui, j + \left(\frac{\partial u}{\partial x}\right)_{i,j} \Delta x + \left(\frac{\partial^2 u}{\partial x^2}\right)_{i,j} \frac{(\Delta x)^2}{2} + \left(\frac{\partial^3 u}{\partial x^3}\right)_{i,j} \frac{(\Delta x)^3}{6} + \cdots - \frac{ui+1,j-ui,j}{\Delta x}$$

$$O(\Delta x) = ui + 1, j = ui - 1j + 2\left(\frac{\partial u}{\partial x}\right)_{i,j} \Delta x + 2\left(\frac{\partial^3 u}{\partial x^3}\right)_{i,j} \frac{(\Delta x)^3}{6} + \cdots \quad (3.8)$$

The RHS of equation (3.8) can be expressed as

$$\left(\frac{\partial u}{\partial x}\right)_{i,j} = \frac{ui+1,j-ui-1,j}{2\Delta x} O(\Delta x)^2 \quad (3.9)$$

The equation (3.9) is referred to as the second-order central difference.

The same procedure underlies the expression for the *y*-derivative obtained following same procedures and the outcome like that of the *x* derivatives

$$\left(\frac{\partial u}{\partial x}\right)_{i,j} = \frac{ui+1,j-ui,j}{\Delta y} O(\Delta y) \quad \text{Forward difference} \quad (3.10)$$

$$\left(\frac{\partial u}{\partial x}\right)_{i,j} = \frac{ui,j-u-1j}{\Delta y} O(\Delta y) \quad \text{Backward difference} \quad (3.11)$$

$$\left(\frac{\partial u}{\partial x}\right)_{i,j} = \frac{ui+1,j-ui-1,j}{2\Delta y} O(\Delta y)^2 \quad \text{Central difference} \quad (3.12)$$

The first-order-accurate equations as expressed above are apparently inadequate to solve the broad spectrum of flowfield variables in fluid dynamics. This takes us to revisiting the governing equations for the inviscid (Euler equations)

The first-order-accurate equation as above suffices for the inviscid fuels such as DPK and Hydrogen.

STEP 9. Solution initialisation – depend on the solver (Steady State and Transient State). This is because the occurrence of flows is complex and non-linear. Several iteration processes were undertaken before to observe simulation consistency and ultimately convergence.

STEP 10. Retrieving Result of interest - (Distribution of flow rate, temperature, power and heat, pressure) and plots for respective parameters

STEP 11. Plots were retrieved per parameter per equivalence ratio for each of the fuels and analysed. Plots of fuels exhibiting same characteristics across classifications were discounted while retaining those exhibiting different characteristics. Details were subsequently obtained from each plot and contours maps and translated in tabular formats

RESULTS AND DISCUSSION

Table 6 show DPK/Kerosene combusted at 0.3φ presented the highest dynamic pressure of 874kPa at 60cm downstream combustor with subsequent declination across equivalence ratios with increasing equivalence ratio. The general temperature distribution at 0.3φ was observed to be the highest; this was closely followed by readings at 0.5φ, 0.7φ and 0.9φ.

Table 6: Dynamic Pressure Profile across equivalence ratios for DPK Combustion

Length within Combustor(m)	0.3φ	0.5φ	0.7φ	0.9φ
0	451,852.00	165,385.00	83,824.00	49,455.00
0.2	325,926.00	115,385.00	60,294.00	37,455.00
0.4	196,296.00	69,231.00	36,029.00	22,182.00
0.6	874,074.00	315,152.00	161,765.00	97,455.00

Table 7 shows the total temperature profile across equivalence ratios obtained during the simulation of DPK/Kerosene. The temperature reading at 0.3φ shows similarity in the profile structure across combustor with same temperature characteristics were exhibited at higher equivalence ratios considered for the simulation process. The temperature profile showed consistency in a flame temperature across all equivalence ratios with 1042.53-1045.15 (Table 7). This amply suggests a moderate flame temperature range. The high temperatures were observed in the combustor reaction zone along the combustor axis.

Table 7: Total Temperature Profile across equivalence ratios for DPK Combustion

Length within Combustor(m)	0.3φ	0.5φ	0.7φ	0.9φ
0	1,044.12	1,044.59	1,044.41	1,042.53
0.2	1,044.59	1,044.85	1,044.82	1,042.94
0.4	1,044.71	1,045.15	1,045.00	1,043.09
0.6	1,044.81	1,045.29	1,045.18	1,043.24

The total pressure readings obtained from the investigation showed that highest pressure distribution across all equivalence ratios occurred at 0.3φ, with the least profile distribution occurring at 0.9φ. (Table 8). It further revealed the progressive decline in pressures with increasing equivalence ratio values, but consistency in growth from ignition point through increase at 20cm downstream combustor to drop at the region of unsteady combustion zone with the further surge downstream combustor

Table 8: Total Pressure Profile across equivalence ratios for DPK Combustion

Length within Combustor(m)	0.3φ	0.5φ	0.7φ	0.9φ
0	351,852.00	130,769.00	65,385.00	41,818.00
0.2	500,000.00	182,051.00	93,590.00	57,273.00
0.4	388,889.00	138,462.00	73,077.00	43,636.00
0.6	370,370.00	312,821.00	160,256.00	97,500.00

CONCLUSION

The highest DPK Dynamic pressure occurred at 0.3φ at upstream combustor with subsequent declination downstream across all equivalence ratios on the incremental variation of the equivalence ratio. The Total Pressure exhibited same characteristics. The highest Dynamic Pressure of 874kPa occurred downstream (0.6m) downstream combustor. The temperature profile showed consistency across all equivalence ratios.

The main precipitance of combustion instability and combustion noise is credited with the application of the LP Combustor to lower combustion temperatures, a process encouraged by the premixing of the fuel and the oxidiser [8], [1]; [11]. [16] stated that the highest temperatures during combustion are obtained upstream combustor (near nozzle). The temperature of hydrogen gas was 2330K and the natural gas 2290k[20]. On the other hand, [12] in their work obtained 1850k and had argued against the theoretical temperature of 1950k. The various temperature profiles as obtained by this study showed explicitly what was obtainable at various equivalence ratios and correlates with the work of [16] and [16]. [15] in their work stated that the gas turbine exhaust temperatures hoover around 2073.15K-2273.15k, which they considered too hot for the nozzle guide vanes of the turbine. The DPK fuel was observed to exhibit consistency in a flame temperature range between 1042.53-1045.15 at all equivalence ratio considered. This amply suggests a moderate flame temperature range. These high temperatures were observed in the combustor reaction zone along the combustor axis. The lower temperature positions DPK as easily susceptible to combustion instability occurrence, and less prone to the formation of pollutants. The combustion data would however enable the design of DPK fuel specific LP Combustor with applicable Wireless Sensory System (WST) along with combustor supervisory control and data acquisition system (SCADA) for sensing and predicting temperature in excess of 1033.15K, which would trigger the incoming fuel /air ratio (equivalence ratio) to avert the occurrence of thermoacoustic instabilities.

ACKNOWLEDGMENT

Profound gratitude to BSN Nigeria allowing the use of the facility for private research and write-ups.

REFERENCES

[1] W.A. Chishty, and M. Klein, "Combustion and Emission issues in Gas Turbines". http://www.iagtcommittee.com/downloads/2009papers/Training%20Session2%20-%20Combustion%20Issues%20in%20Gas%20Turbines. 2009.

[2] Clean Air Technology Centre, "Nitrogen Oxides(NOx), Why and How they are Controlled", EPA Technical Bulletin 456/F-99-006R November. 1999.

[3] F.C Culick, and V. Yang, "Overview of Combustion Instabilities in Liquid - Propelled Rocket Engines". http://core.ac.uk/download/pdf/4886871.pdf. 1995.

[4] F.C. Culick, "Combustion instabilities in liquid-fueled propulsion systems", *Paper reprinted from conference proceedings No. 450 Advisory Group for Aerospace Research & Development AGARD*. http://www. authors.library.caltech.edu/22028 /. 2012

[5] A. Dowling, "The Calculations of Thermoacoustic Oscillations". *Journal of Sound and Vibrations* (1995) 180(4), 557-58

[6] S. Ducruix, T. Schuller, D. Durox, and S. Candel, "Combustion Instability Mechanisms in Premixed Combustors". *Combustion Instabilities in Gas Turbine Engines: Operational Experience, Fundamental Mechanisms and Modelling*. T. Lieuwen and V. Yang eds., Progress in Aeronautics and Aeronautics Series, Vol. 210. AIAA, pp.179-212, 2005

[7] T. Lieuwen, "Investigation of Combustion Instability Mechanisms in Lean Premixed Gas Turbines". PhD Thesis, Dept. of Mechanical Engineering. Georgia Institute of Technology Georgia, California.1999

[8] T. Lieuwen, H. Torres, C. Johnson, and B. Zinn, "A Mechanism of Combustion Instability in Lean Premixed Gas Turbine Combustors" *Journal of Engineering for Gas Turbines and Power*, Vol. 123, No 1, 2001, pp.182-190. 2001.

[9] T. Lieuwen, "Modelling Premixed Combustion-Acoustic Wave Interactions: A review". *Journal of Propulsion and Power Vol. 19, No 5 September-October 2003*.

[10] T. Lieuwen and B.T. Zinn, "The Role of Equivalence Ratio Oscillations in Driving Combustion Instabilities in Low NOx

Gas Turbines". *Proceedings of the Combustion Institute, Vol 27, The Combustion Institute Inst., Pittsburgh, PA*, pp. 1809-1816. 1998

[11] L. Merotto, M. Sirignano, M. Commodo, A. D'Anna, R. Donde, and S. De Iuliis, "Experimental Characterization and Modelling for Equivalence Ratio Sensing in Non-Premixed Flames using Chemiluminescence and Laser-Induced Breakdown Spectroscopy Techniques". Energy Fuels, 2017, 31 (3), pp 3227–3233.

[12] F.H. Pathan, N.K Patel and M.V. Tadvi, "Numerical Investigation of the Combustion of the Methane-Air Mixture in Gas Turbine Can-Type Combustion Chamber". *International Journal of Scientific & Engineering Research*. Volume 3, Issue10, October-2012 ISSN-2229-5518.

[13] W. Polifke, "Combustion instabilities". *VKI Lecture Series Journal of Advances in Acoustics and Applications* March 15th – 19th, Brussels Belgium

[14] S. Pawar, A. Seshadri, V. Unni and R. Sujith "Thermoacoustic Instability as Mutual Synchronisation between the Acoustic Field of the Confinement and Turbulent Reactive Flow" Journal *of Fluid Mechanics.Vol.*827, pp.664-693. 2017 doi:10.1017/jfm.2017.438

[15] A. Trifan and A. Pruiu "Technologies used on Maritime Boilers for the Reduction of NOx Emissions". Bulletin of the Transilvania University of Brasov. Vol. 2(51)-2009 Series 1: Engineering Sciences. 2010

[16] H. Tomczak, G. Benelli, L. Carai and D. Cecchini "Investigation of A Gas Turbine Combustion System Fired with Mixtures of Natural Gas and Hydrogen". *IFRF Combustion Journal, Dec. 2002*, 19 pp. Article ID 200207

[17] D. You, V. Yang and X. Sun (2003). "Three-Dimensional Linear Stability Analysis of Gas Turbine Combustion Dynamics" T. Lieuwen, and V. Yang eds., *Combustion Instabilities in Gas Turbine Engines: Operational Experience, Fundamental Mechanisms and Modelling*. Progress in Aeronautics and Aeronautics Series, Vol. 210. AIAA. 417-448. 2005

[18] W. Alli, O. Ighodalo and C. Ajuwa "The effect of equivalence ratios variation in gas turbine fuel types during combustion instabilities". *International Journal of Scientific and Engineering Research*. Vol. 9 Issue 3 March 2018

[19] D. Conner. "Combustion characteristics of propane: effect of equivalence ratio on flame structure and colour, Liftoff and flashback phenomena, flame propagation speed, detonation, and critical number". www. danielconner.weebly.com/.../combustion_characteristics_of_propane_lab_report.pdf. 2011

[20] W. Alli," Numerical Analysis of Fuel Types During Combustion Instabilities in Gas Turbine Engine Lean Premixed Combustor" Unpublished PhD Thesis, Dept. of Mechanical Engineering, Faculty of Engineering & Technology. Ambrose Alli University, Ekpoma Edo state. 2018.

[21] J. Rayleigh. "The theory of sound". https://www.irphe.univ-mrs.fr/.../Rayleigh/N0095130. 1877

[22] W. Alli, O. Ighodalo and C. Ajuwa "MRO and Design Parameters Determination for Improving Availability and Reliability of GTEs equipped with LP Combustors" under the review of *Nigerian Journal of Technological Development*

[23] H. Lee., "Combustion Instability Mechanisms in A Lean Premixed Gas Turbine Combustor". PhD thesis. College of Engineering, Pennsylvania State University. 2009

[24] W. Alli, O. Ighodalo and C. Ajuwa "Combustion Characteristics Comparison of Kerosene and Methane Fuels During Combustion Instabilities in Gas Turbine Lean Premixed Combustors" Under the review of *Research Journal of Applied Sciences, Engineering and Technology*

[25] B. Zinn., and Lieuwen "Combustion Instabilities: Basic Concepts, *Combustion Instabilities in Gas Turbine Engines: Operational Experience*, *fundamental mechanisms, and Modelling.* T.C Lieuwen, and V. Yang. (eds), Progress in Aeronautics and Astronautics Series, Vol. 210, AIAA, 3-24. 2005

Authors

· Wilson Alli is currently pursuing doctorate programme in Mechanical Engineering Department Ambrose Alli University, Ekpoma Edo State Nigeria Phone: +234(0)8080175708. Email: wilsalli@gmail.com

· Prof. Osagie Ighodalo is of the Mechanical Engineering Department Ambrose Alli University, Ekpoma Edo State Nigeria. Phone: +234(0)8033626385. Email: oighodalo@yahoo.com

· Prof. Christopher Ajuwa is of the Mechanical Engineering Department Federal University of Petroleum Resources Effurun-Warri Delta State Nigeria Phone: +234(0)8055515958. Email: ajuwa.christopher@fupre.edu.ng